Liquid Crystals

ISSN: 0267-8292 (Print) 1366-5855 (Online) Journal homepage: https://www.tandfonline.com/loi/tlct20

Synthesis and mesophase behaviour of branched azobenzene-based supramolecular hydrogen-bonded liquid crystals

Wan-Li He, Han Gu, Peng Zhao, Zhou Yang, Hui Cao & Dong Wang

To cite this article: Wan-Li He, Han Gu, Peng Zhao, Zhou Yang, Hui Cao & Dong Wang (2017) Synthesis and mesophase behaviour of branched azobenzene-based supramolecular hydrogen-bonded liquid crystals, Liquid Crystals, 44:3, 593-602, DOI: 10.1080/02678292.2017.1306635

To link to this article: https://doi.org/10.1080/02678292.2017.1306635

Published online: 29 Mar 2017.

LIQUID CRYSTALS, 2017
VOL. 44, NO. 3, 593–602
https://doi.org/10.1080/02678292.2017.1306635

Taylor & Francis
Taylor & Francis Group

ARTICLE

Synthesis and mesophase behaviour of branched azobenzene-based supramolecular hydrogen-bonded liquid crystals

Wan-Li He, Han Gu, Peng Zhao, Zhou Yang, Hui Cao and Dong Wang

Beijing Key Laboratory of Function Materials for Molecule & Structure Construction, School of Materials Science and Engineering, University of Science and Technology Beijing, Beijing, P. R. China

ABSTRACT

Five types of new pyridine-based azo compounds, namely, 4-(4′-pyridylazo)-4′′-alkoxybenzoates or 4-(4′-pyridylazo)-4′′-substituted benzoates with straight or branch terminal were prepared as hydrogen bond (H-bond) acceptors to build mesogens. After self-assembled with different carboxylic acids, the resulted H-bond complexes were confirmed for the stability of H bond by fourier transform infrared spectroscopy (FTIR) spectroscopy, and investigated for the mesophase behaviour by differential scanning calorimetry and polarised optical microscopy. The influence of terminal chains in azo accepter or acid donor and the structure of acid donors on the mesogenic behaviour were discussed in detail.

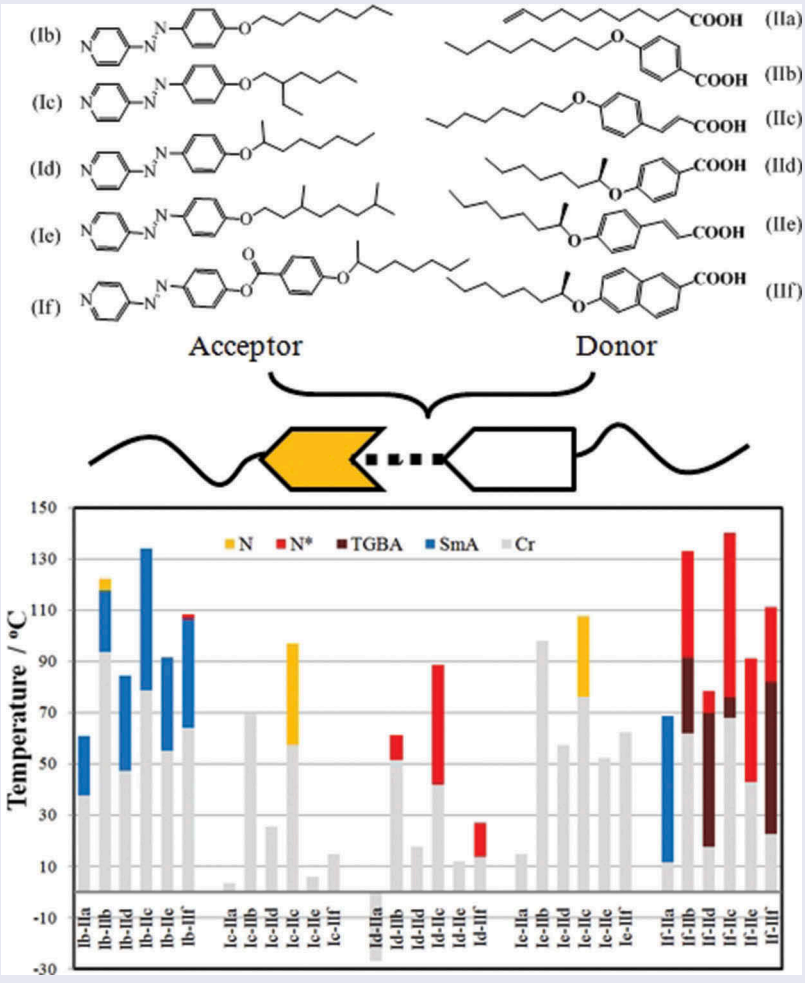

ARTICLE HISTORY
Received 10 February 2017
Accepted 10 March 2017

KEYWORDS
Hydrogen-bonded; liquid crystal; azobenzene; chiral; branched

CONTACT Wan-Li He hewanli@mater.ustb.edu.cn

1. Introduction

Liquid crystals are unusual molecules which could exist in an intermediate state of matter termed the liquid crystalline (LC) state in which the material is fluid like a liquid, but the molecules possess an overall orientational order like in a crystalline solid. There are many kinds of LC materials classified on the structures (rod-shape, banana-shape and disc-shape) and the connecting bond for the formation of LC mesogens (covalent-bonded, non-covalent bonded). Calamitic LC as the most common ones usually consists of a rigid mesogenic core connected to a flexible tail with covalent bonds, and are widely used in a flat-panel display, smart windows, laser and other photonics.

Besides covalent bonding, hydrogen bonding has been used to assemble the mesogenic core of calamitic LCs giving rise to the facile field of hydrogen bonded (H-bonded) LCs. With the facileness of self-assembly preparation and the convenience to adjust composition of the H-bond precursors, many functional materials and devices could be easily obtained by through solvent dissolving or heating or mechanical grinding the H-bond precursors without conventionally time-consuming and expensive chemical synthesis [1–3]. The simplest examples of H-bonded LCs are p-alkoxy benzoic acid homodimers in which the rigid mesogenic cores are formed by head-to-head hydrogen intermolecular bonding [4]. In H-bonded LC heterodimers, the rigid mesogenic core is formed by the H-bond between a donor and an acceptor. For example, the intermolecular N–HO H-bonded mesogen could be built from 4-alkoxybenzoic acid vs. isonicotinate or nicotinate derivative [5,6], 4-alkoxybenzoic acid vs. 4-alkylpyridine [1,7] or 4-alkoxylpyridine [8], 4-alkoxybenzoic acid vs. bipyridyl compound [9,10], 4-alkoxybenzoic acid vs. heptyl p-hydroxy benzoate [11], 4-alkoxyphenol vs. 4-alkylpyridine [12,13] and multiple H-bonding [14,15]. The intermolecular H-bonds were thus widely used for the inducting LC both in the low-molecular-weight system [16] and in the side chain of polysiloxanes [17]. The textures and phase transition temperatures of the LC phases in these hydrogen-bonded heterodimers depend on the identities of the H-bond donors and acceptors.

On the other hand, as is well known, azobenzenes have the unique feature of reversible trans–cis isomerisation upon light irradiation [18], which can cause the large conformational and polarisation changes intramolecularly. The trans-form of azobenzene has a rod-like structure that can stabilise the LC superstructure, whereas its cis-form is bent-like structure and generally destabilises the LC superstructure by generating disorder in the aligned systems. Therefore, the azobenzene moiety is the most widely used photoactive bistable group whether in a rod-shaped [19] or bent-core-shaped mesogen [20,21] because of its easy synthesis and having a good compatibility with LC phase especially in its trans-form (its elongated structure). Depending on the *trans–cis* transformation of azobenzene, extensive works have been performed to control the orientation of LC, such as inducing nematic phase [18], smectic phase [22], cubic phases [23], adjusting the reflection wavelength of the chiral nematic (N*) phase [24–27] or Bragg reflection of BPs [28–33], phase transitions from nematic to isotropic states [34] and the helical twisting power [35,36]. However, azo compounds usually have relatively high melting point and low solubility in liquid crystals matrix, which has been one of the obstacles to their potential applications. To explore the potential use of the azobenzene liquid crystals, the H-bonded complexes have been designed to induce room temperature mesophases. Herein, five types of pyridine-based azobenzene compound, namely, 4-(4′-pyridylazo)-4″-alkoxybenzoates or 4-(4′-pyridylazo)-4″-substituted benzoates were prepared as H-bond acceptors, and six types of carboxylic acids with different structure were used as H-bond donors. The flexible terminal chain of azo accepter or acid donor was changed from straight chain to branched chain, and the rigid core of the H-bonded complex was changed from two rigid rings to five rigid rings in the structure to study the effect of structure on the mesogenic properties of azobenzene-based H-bonded complexes, as shown in Figure 1.

2. Experimental

2.1. Characterisation

Infrared spectra were recorded by using a Nicolet 510P FTIR spectrometer. ^{1}H NMR and ^{13}C NMR spectra on Bruker AV400 instrument in DMSO and $CDCl_3$. The mesogenic properties were studied through an Olympus BX-51 Polarizing Optical Microscope (POM) equipped with a Linkam Scientific LTS 350 heating/freezing stage. For Differential Scanning Calorimetry (DSC), a Perkin-Elmer DSC 6 instrument was used, and the scanning rate was 10°C/min, the samples were sealed in aluminum capsules in the air, and the holder atmosphere was dry nitrogen.

2.2. Synthesis

Chemicals used in this work were commercially available from ACROS Company and from Beijing

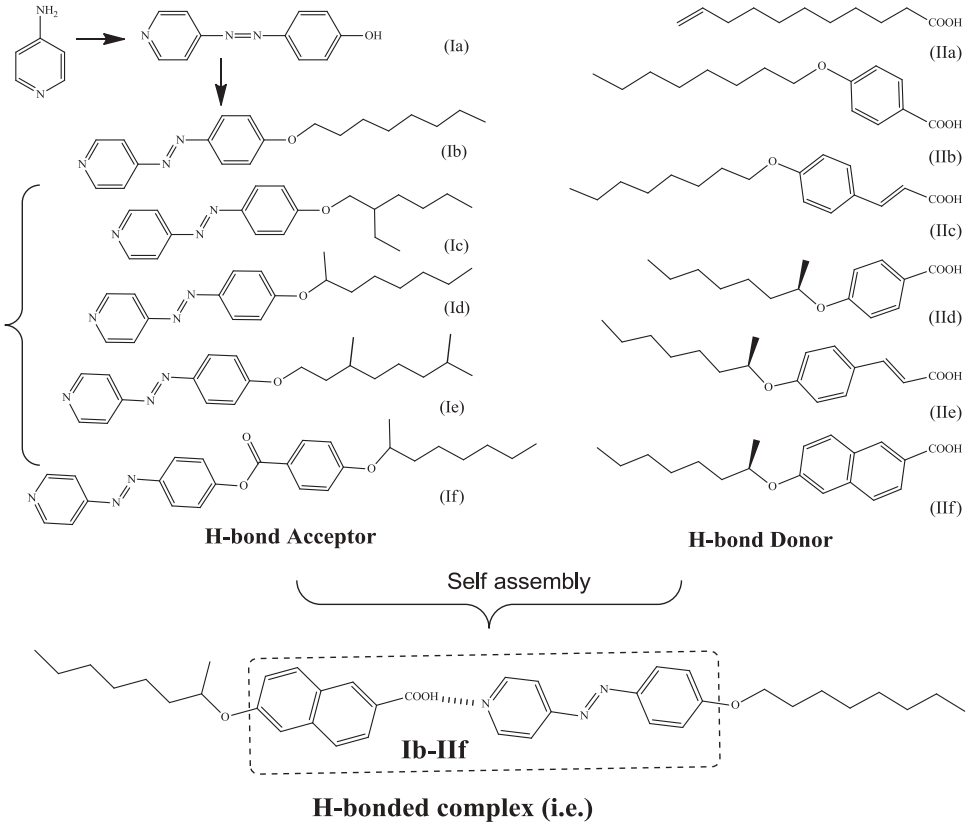

Figure1. Synthetic routes of azobenzene precursors and the structure of H-bond donors.

Chemical Product Factory, and used without further purification. The synthesis of H-bond precursors and the H-bonded complexes was based on the route of Figure 1 and obtained by the similar procedures reported [37–39]. The procedures of complexes were summarised analogously to the preparation of ***Ib-IIf*** as shown.

2.3 Synthesis of 4-(4-hydroxyphenylazo) pyridine (Ia)

A 10 wt% NaOH aqueous solution (20 mL) including sodium nitrate (4.00 g, 58 mmol) and phenol (5.00 g, 53 mmol) was prepared and cooled to 0°C. Subsequently, it was added dropwise to another aqueous solution with HCl 45 mL (25 mL 11 N HCI and 20 mL water) and 4-aminopyridine (6.00 g, 64 mmol). The reaction mixture was stirred under an ice bath (0°C) for 0.5 h. Then, the pH of the reaction mixture was adjusted to pH = 6–7 by addition of a 10 wt% NaOH aqueous solution. A yellow precipitate was collected by filtration. The crude product was washed with water and recrystallised from acetone to give bright yellow solid. Yield 2.96 g (32.6%), Rf = 0.4 (EtOAc/DCM = 1:1). FTIR (KBr, cm^{-1}): 3454 (HO–), 2500, 1590, 1581, 1457, 1403, 1293, 1136, 830, 635, 555. ^{1}H NMR (400 MHz, DMSO, δ): 6.96–6.98 (d, 2H, –O–ArH–), 7.66–7.67 (d, 2H, Ar),7.85–7.87 (d, 2H, pyridine Hs), 8.75–8.76 (d, 2H, –N– pyridine Hs), 10.58 (s, 1H, HO–).

2.4. Synthesis of 4-(4-octyloxyphenylazo) pyridine (Ib)

1-Bromooctane (1.93 g, 10 mmol) was dissolved in actone (20 mL), which was added dropwise to a actone (20 mL) solution of K_2CO_3 (6.90 g, 5 mmol), KI (0.01 g, 0.1 mmol) and 4-(4-hydroxyphenylazo)pyridine (2.00 g, 10 mmol) at 60°C. After 16 h, the mixture was poured into water (200 mL) and then extracted with ethyl acetate (50 mL×3). A rotary evaporator was used to remove all of the solvent. The crude product was purified by silica gel column chromatography with ethyl acetate and petroleum ether (1:2) as eluent to obtain 2.24 g orange powder. Yield: 72%, Rf = 0.4 (EtOAc/petroleum ether = 1:2). FTIR (KBr, cm^{-1}): 2919, 2853 (–CH_2–, –CH_3 stretching), 1584 (Ar stretching), 1504 (Ar–O– stretching), 1467(aromatic C=C), 1408, 1321, 1263, 1144, 1024, 925, 846, 724,

632, 560. ^{1}H NMR (400 MHz, $CDCl_3$, δ): 0.86–0.89 (t, 3H, $-CH_3$), 1.28–1.48 (m, 10H, $-C_5H_{10}-$), 1.79–1.83 (m, 2H, $-CH_2-$), 4.04 (d, 2H, $-O-CH_2-$), 6.99–7.01 (d, J = 9.2 Hz, 2H, –O–ArH–), 7.65–7.66 (d, J = 6.0 Hz, 2H, Ar–H), 7.92–7.95 (d, J = 8.8 Hz, 2H, pyridine Hs), 8.75–8.76 (d, J = 6.0 Hz, 2H, –N– pyridine Hs).

Compounds *Ic*, *Id* and ***Ie*** were synthesised by the analogous procedure used for **compound *Ib*** using 1-bromo-2-ethyl hexane and (R)-2-octanyl tosylate as starting material, respectively.

Compound *Ic*, red wax-like solid, Yield 70%, Rf = 0.5 (EtOAc/petroleum ether = 1:1): FTIR (KBr, cm^{-1}): 2931, 2848 ($-CH_2-$, $-CH_3$ stretching), 1601, 1499, 1404, 1256, 1146, 1012, 842, 563. ^{1}H NMR (400 MHz, DESO, δ): −3.85 to −3.80 (m, 6H, $-CH_3$,$-CH_3$), −3.44 to −3.17 (m, 2H, methylene; 6H, $-C_3H_6-$), −3.01 to −2.98 (m, 1H, methyne), −0.83 to −0.81 (d, J = 6.0 Hz, 2H, $-O-CH_2-$), 2.25–2.27 (d, J = 8.8 Hz, 2H, –O–ArH–), 2.89–2.90 (d, J = 6.0 Hz, 2H, Ar–H), 3.17–3.20 (d, J = 8.8 Hz, 2H, pyridine Hs), 4.00–4.01 (d, J = 6.0 Hz, 2H, –N– pyridine Hs).

Compound *Id*, orange-red liquid, Yield 80%, Rf = 0.3 (EtOAc/petroleum ether = 1:3): FTIR (KBr, cm^{-1}): 2930, 2852 ($-CH_2-$, $-CH_3$ stretching), 1600, 1497, 1404, 1254, 1141, 942, 842, 631, 563. ^{1}H NMR (400 MHz, DMSO, δ): −3.90 to −3.88 (t, 3H, $-(CH_2)_5\underline{CH_3}$), −3.47 to −3.13 (m, 8H, methylene; 3H, $-CH_3$), −3.06 to −2.98 (m, 2H, $-CH(CH_3)-\underline{CH_2}-$), −0.30 to −0.26 (m, J = 18.4 Hz, 1H, $-O\underline{CH}(CH_3)-CH_2-$), 2.22–2.23 (d, J = 8.8 Hz,2H, –O–ArH–), 2.89–2.90 (d, J = 6.0 Hz, 2H, –Ar–H), 3.16–3.18 (d, J = 8.8 Hz, 2H, pyridine Hs), 3.99–4.01 (d, J = 5.6 Hz, 2H, –N– pyridine Hs).

Compound *Ie*, orange-red liquid, Yield 80%, Rf = 0.5 (EtOAc/petroleum ether = 1:1): FTIR (KBr, cm^{-1}): 2927, 2868 ($-CH_2-$, $-CH_3$ stretching)1583, 1500, 1420, 1256, 1144, 1011, 845, 561. ^{1}H NMR (400 MHz, $CDCl_3$, δ): 0.85–0.86 (m, 6H, $-CH_3$,$-CH_3$), 0.94–0.95 (m, 3H, $-CH_3$),1.28–1.48 (m, 10H, $-C_5H_{10}-$), 4.05–4.10 (d, J = 20.4 Hz, 2H, $-O-CH_2-$), 6.99–7.24 (d, J = 8.8 Hz, 2H, –O–ArH–), 7.65–7.67 (d, J = 6.4 Hz, 2H, Ar–H), 7.92–7.95 (d, J = 8.8 Hz, 2H, pyridine Hs), 8.74–8.76 (d, J = 4.0 Hz, 2H, –N– pyridine Hs).

2.5. Synthesis of 4-(4-hydroxyphenylazo) pyridine 4-(octan-2-yloxy) benzoate (If)

A mixture of 4-(4-hydroxyphenylazo) pyridine (0.40 g, 2.0 mmol), (S)-4-(octan-2-yloxy)benzoic acid (0.5 g, 2.0 mmol), 4-(N,N-dimethylamino) pyridine (DMAP) (0.12 g, 1.0 mmol) and N-ethyl-N′-(3-dimethylaminopropyl) carbodiimide hydrochloride (EDC) (1.0 g, 5 mmol) was added in dry dichloromethane (100 ml) and stired for 20 h at room temperature. After filtering off the precipitate, the solvent was removed under reduced pressure and the red residue was purified by column chromatography on silica gel to give yellow solid (0.7 g). Yield 81%, Rf = 0.4 (EtOAc/petroleum ether = 1:2). FTIR (KBr, cm^{-1}): 2930, 2854 ($-CH_2-$, $-CH_3$ stretching), 1740 (C=O stretching), 1605, 1509, 1405, 1261, 1172, 1062, 836, 760, 561. ^{1}H NMR (400 MHz, DMSO, δ): −3.90 to −3.88 (t, 3H, $-(CH_2)_5CH_3$), −3.51 to −3.32 (m, 8H, methylene; 3H, $-CH_3$), −3.17 to −2.99 (m, 2H, –CH $(CH_3)-\underline{CH_2}-$), −0.29 to −0.25 (m, J = 17.6 Hz, 1H, $-\underline{CH}(CH_3)-CH_2-$), 2.212 (d, 2H, $-CH(CH_3)-O-\underline{ArH}-$), 2.63–2.65(d, J = 8.4 Hz, 2H, O=C–O–ArH–), 2.94–2.96 (d, J = 5.6 Hz, 2H, O=C–O–ArH–), 3.27–3.30 (d, J = 8.8 Hz, 2H, pyridine Hs), 3.71–3.39 (d, J = 8.8 Hz, 2H, O=C–ArH–), 4.04–4.06 (d, J = 6.0 Hz, 2H, –N– pyridine Hs).

2.6. Synthesis of the hydrogen-bonded complexes

All the H-bonded complexes dealt with in this study were prepared similarly to the method of complex ***Ib–IIf*** shown as follows. The requisite amounts of ***Ib*** and ***IIf*** were dissolved in tetrahydrofuran and followed by slowly removing the solvent under reduced pressure. The resulting solid complex was dried in vacuum at room temperature for about 24.0 h.

3. Results and discussion

3.1. FTIR spectra

The formation of H-bonds in complexes, as shown in Figure 2, was confirmed by IR. The IR spectra of acid ***IIf*** showed an associated characteristic stretching band (approximately from 2500.0 cm^{-1} to 3200.0 cm^{-1}) resulting from dimerised carboxylic acid and a band of C=O stretching of acid ***IIf*** was centred at 1674 cm^{-1}. While in the IR spectra of H-bonded complexes (***Ib–IIf***), the band of C=O stretching shifted to 1695 cm^{-1}. The broad band of dimerised carboxylic acid disappeared and two new emerging bands appeared at 2450 and 1930 cm^{-1}, which identified the presence of H-bond between carboxylic acid and pyridyl group in the complexes [40–42]. The similar shift of carbonyl peaks and appearance of two H-bonded bands, had also been found in other complexes. When increasing the length of the terminal chain, the H-bond characteristic bands could obviously be recorded and changed

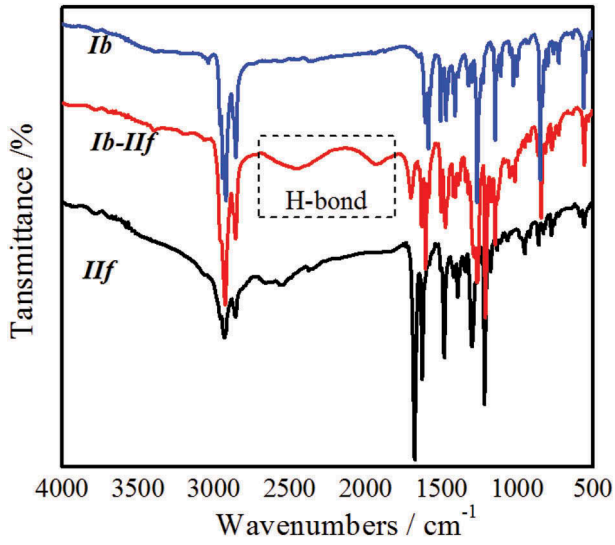

Figure 2. (colour online) FTIR spectra of the precursors and the H-bonded complexes.

little. The stability of the H-bonds could be confirmed by temperature-dependent IR spectra [40–44]. The appearance of two bands centred at 2450 and 1930 cm^{-1} in ***Ib–IIf*** resulted from the formation of H-bonds between carboxylic acid and pyridyl groups (–O–H … N) and changed little within the clear point of ***Ib–IIf*** (below 160.0°C) as shown in Figure 3a. Additionally, the stability of the H-bonds was also confirmed by UV-irradiation-dependent IR spectra. The two characteristic bands of carboxylic acid and pyridyl groups (–O–H … N) changed little with 365 nm UV-irradiation (15 mW/cm^2) as shown in Figure 3b, and thus indicated a well stability of H-bond in the H-bonded complexes.

3.2. Thermal and phase behaviours

The thermal behaviours of H-bond precursors and H-bond complexes were investigated by using the DSC measurement and POM observation, the phase transition temperature of azo precursors and the complexes was listed in Table 1 and Table 2. It was found that only the acids ***IIb*** and ***IIc*** showing mesophase and no mesogenic properties were observed in the other acids and azo compounds. The melting or clearing points of the precursors increased with increasing rigid structure length, but decreased with the introduction of the terminal alkyl chain structure.

The mesogenic behaviours of H-bonded complexes were different from that of the H-bond precursors and were also investigated by using the DSC measurement and POM observation. The phase transition temperature of azo compounds ***Ib, Ic, Id, Ie, If*** and the corresponding H-bonded complexes were summarised in Tables 1 and 2, respectively. For

Table 1. The phase transition temperatures and the enthalpies of the H-bonded precursors.

Comp.	Transition temperature (°C)	Comp.	Transition temperature (°C)
Ia	Cr 259.2 (128.9) I (Lit. 260°C) [18]	***IIa***	Cr 20.8 (63.5) I
Ib	Cr 65.8 (107.2) I (Lit. 70.6°C [23], 67°C [45])	***IIb***	Cr 104.2 (39.3) SmC 109.3 (3.7) N 149.1 (13.7) I (Lit. Cr 101 SmC 107 N 147°C) [46]
Ic	Cr 37.8 (61.8) I	***IIc***	Cr 146.0 (66.2) N 175.3(9.1) I (Lit. 150°C) [47]
Id	Cr 32.8 (30.6) I	***IId***	Cr 67.2 (61.88) I [38]
Ie	Cr 48.3 (34.0) I	***IIe***	Cr 81.2 (71.5) I [38]
If	Cr 86.1 (57.9) I	***IIf***	Cr 100.1 (13.2) I [37]

Cr: Crystalline, SmC: smectic C phase, N: nematic phase, I: isotropic liquid.

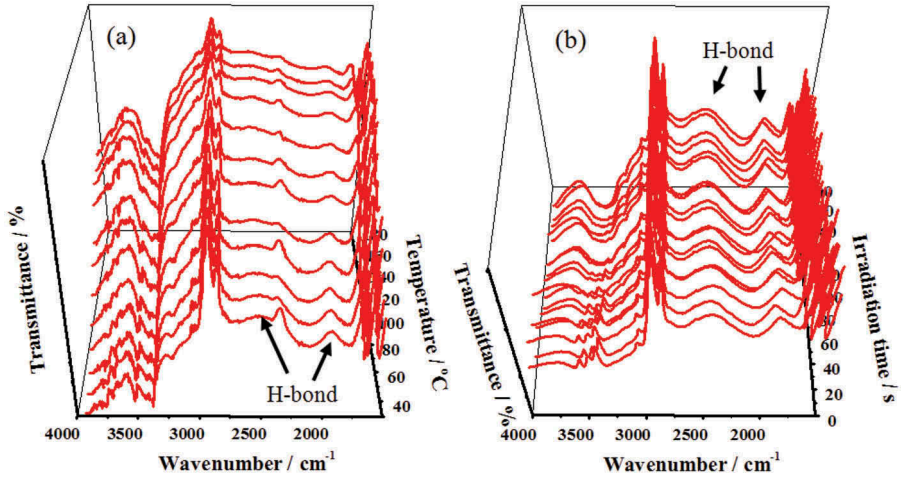

Figure 3. (colour online) FTIR spectra of ***Ib–IIf*** during the heating (a) and UV-irradiating (b).

Table 2. The phase transition temperatures and the enthalpies of the H-bonded complexes.

Complex	Transition temperature (°C) and enthalpy (J/g) during heating	Transition temperature (°C) and enthalpy (J/g) during cooling
Ib–IIa	Cr 65.5 (64.8) I	I 60.8 (−18.4) SmA 37.8 (−39.2) Cr
Ib–IIb	Cr 102.8 (39.2) SmA 120.6 (2.2) N 125.1 (1.4) I	I 122.3 (−1.5) N 117.7 (−2.3) SmA 93.6 (−41.6) Cr
Ib–IIc	Cr 96.6 (72.9) SmA 135.7 (3.8) I	I 134 (−4.6) SmA 78.6 (−73.1) Cr
Ib–IId	Cr 63.4 (36.2) SmA 89 (11.9) I	I 84.4 (−11.1) SmA 47.2 (−28.5) Cr
Ib–IIe	Cr 76 (44.7) SmA 95.1 (8.7) I	I 91.6 (−9.8) SmA 55.2 (−39.7) Cr
Ib–IIf	Cr 83.1 (37.2) SmA 109.1 (0.4) N* 110.8 (0.4) I	I 108.4 (−0.3) N* 106.7 (−0.9) SmA 64.2 (−35.5) Cr
Ic–IIa	Cr 21.6 (69.6) I	I 3.61 (−67.8) Cr
Ic–IIb	Cr 81.6 (62.6) I	I 69.3 (−51.4)
Ic–IIc	Cr 69.6 (14.9) N 106.5 (1.2) I	I 97 (−4.5) N 57.3 (−15.7) Cr
Ic–IId	Cr 48.6 (43.3) I	I 25.5 (−42.7) Cr
Ic–IIe	Cr 47.9 (66.9) I	I 5.86 (−32.1) Cr
Ic–IIf	Cr 69.2 (67.7) I	I 14.9 (−33.0) Cr
Id–IIa	Cr 16.1 (68.7) I	I −26.9 (−50.6) Cr
Id–IIb	Cr 65.6 (37.9) N* 73.1 (0.6) I	I 61.4 (−0.4) N* 51.6 (−33.1) Cr
Id–IIc	Cr 58.5 (16.7) N* 94.4 (0.9) I	I 88.6 (−1.0) N* 41.9 (−13.9) Cr
Id–IId	Cr 49.4 (43.5) I	I 17.9 (−46.3) Cr
Id–IIe	Cr 41.4 (35.2) I	I 12.2 (−33.9) Cr
Id–IIf	Cr 45.5 (49.7) I	I 26.9 (−1.3) N* 13.9 (−21.5) Cr
Ie–IIa	Cr 29.7 (28.9) I	I 14.8 (−32.7) Cr
Ie–IIb	Cr 105.9 (56.7) I	I 97.9 (−56.3) Cr
Ie–IIc	Cr 90.8 (31.3) N 112 (1.8) I	I 107.5 (−1.4) N 76.3 (−39.5) Cr
Ie–IId	Cr 65.9 (41.1) I	I 57.3 (−45.0) Cr
Ie–IIe	Cr 64.5 (40.0) I	I 52.3 (−42.8) Cr
Ie–IIf	Cr 70.5 (25.4) I	I 62.2 (−29.0) Cr
If–IIa	Cr 39.9 (20.6) SmA 71.4 (10.2) I	I 68.7 (−6.0) SmA 11.6 (−12.5) Cr
If–IIb	Cr 68.1 (19.1) TGBA* 94.6 (1.3) N* 135.6 (1.5) I	I 132.8 (−2.0) N* 91.7 (−1.2) TGBA* 61.8 (−27.3) Cr
If–IIc	Cr 101.4 (58.1) N* 142.5 (2.4) I	I 140.1 (−2.7) N* 75.8 (−0.7) TGBA* 67.9 (−26.6) Cr
If–IId	Cr 32.2 (24.2) TGBA* 72.3 (0.2) N* 81.6 (1.3) I	I 78.3 (−1.4) N* 69.7 (−0.2) TGBA* 17.7 (−19.7) Cr
If–IIe	Cr 59.1 (41.3) N* 94 (1.7) I	I 91.3 (−1.7) N* 43 (−14.7) Cr
If–IIf	Cr 83.8 (44.1) TGBA* 115.7 (2.4) I	I 111.1 (−2.1) N* 81.8 (−0.3) TGBA* 22.9 (−12.8) Cr

Cr: Crystalline, SmA: smectic A phase, TGBA*: twist ground boundary A phase, N*: chiral nematic phase, N: nematic phase, I: isotropic liquid.

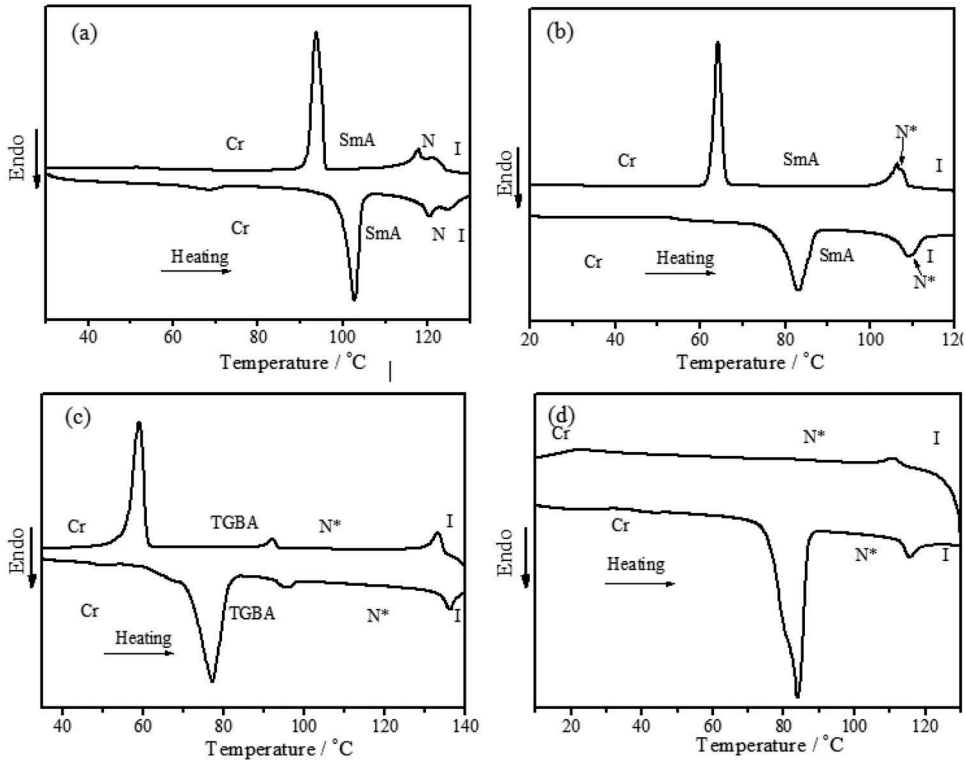

Figure 4. The DSC curve of ***Ib–IIb*** (a), ***Ib–IIf*** (b), ***If–IIb*** (c) and ***If–IIf*** (d).

example, it could be seen from the DSC curve of ***Ib–IIb*** (shown in Figure 4a) that, two endothermic peaks appeared at 105.0°C and 122.6°C during the heating process, respectively, and two exothermic peaks appeared at 120.1°C and 96.9°C during the cooling process, respectively, which imply there was a mesogenic phase between the two temperature peaks. Additionally, one endothermic peak appeared and two exothermic peaks were observed in the DSC curve of ***Id–IIf*** and ***Ib–IIa***, as shown in Figure 4, which indicated these complexes were monotropic LCs. The results of POM observation accorded well with that of DSC measurement during cooling process. From the POM observation, a typical schlieren texture of nematic phase was observed in ***Ic–IIc*** and ***Ie–IIc***, as shown in Figure 5, respectively. A planar oily streak texture of chiral nematic phase was found in ***Id***-derived complexes and higher temperature of ***If***-derived complexes. Additionally, smectic A phase appeared in ***If–IIa*** as well as all the ***Ib***-derived complexes and TGBA phase was found in the ***If***-derived complexes.

Figure 6 showed that the H-bonded LCs with azo mesogen had different mesogenic behaviour on cooling. Mesogenic behaviour was found in all the ***If***-derived complexes and ***Ib***-derived complexes, but only found in some of the branched terminal H-bonded complexes derived from ***Ie, Ic*** and ***Id*** azo acceptors. The phase transition points of the H-bonded complexes were reduced in turn, especially the clearing points and the melting points. A possible explanation for above results is that the length-to-breadth ratio is a key factor to determine the mesogenic behaviour whether in the H-bond LCs or in conventional LCs. When the terminal chain of azo accepter or acid donor was changed from straight chain to branched chain, the length-to-breadth ratio of the resulting H-bonded complexes reduced accordingly, which lead to the phase transition points decreased and mesogenic properties disappeared except the complexes ***Ic–IIc, Ie–IIc, Id–***

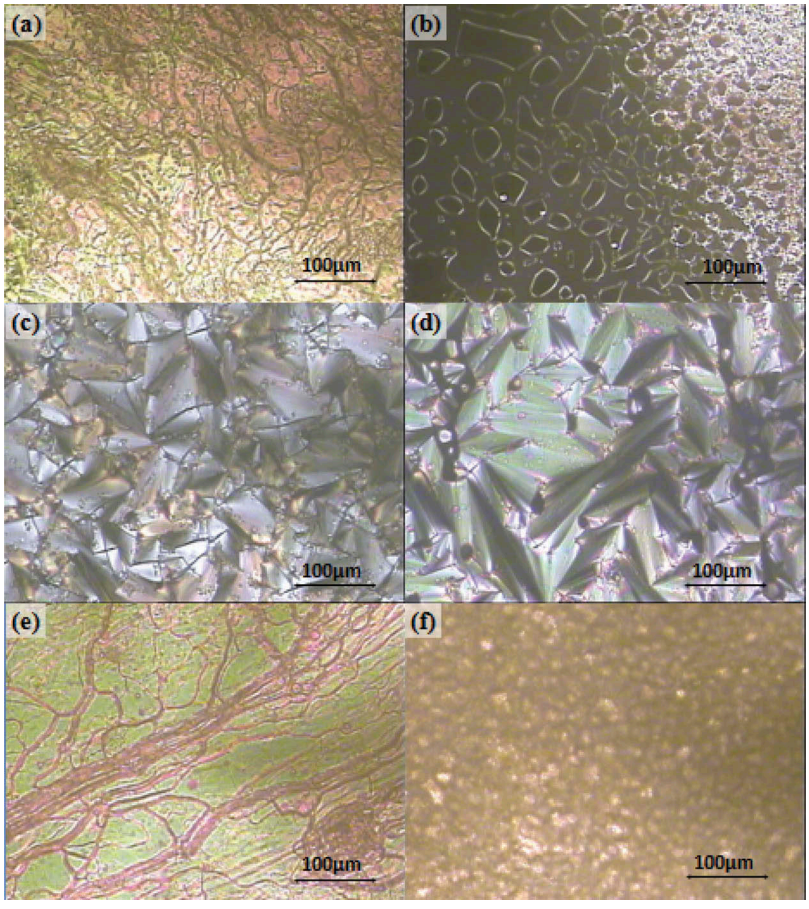

Figure 5. (colour online) Optical textures H-bonded complexes, (a) Planar oily streak texture of chiral nematic phase for complex ***Ib–IIf*** at 114.9°C; (b) Black pseudo-isotropic texture of smectic A phase for complex ***Ib–IIf*** at 111.6°C; (c) SmA phase of ***Ib–IIf*** under homoetropic-oriented condition at 87.3°C (focal conic texture), (d)SmA phase of ***Ib–IIb*** under homoetropic orientation at 122.0°C (fan-shaped texture), (e) Planar oily streak texture of chiral nematic phase for ***If–IIb*** at 114°C; (f) Grid texture of TGBA phase for ***If–IIb*** at 93°C.

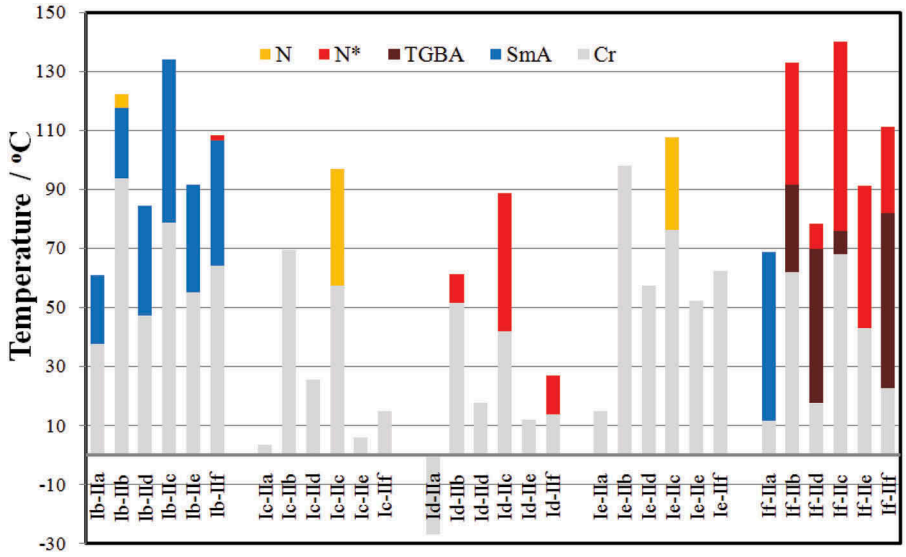

Figure 6. (colour online) The phase transition on cooling for the H-bonded complexes.

IIc, ***Id–IIb*** and ***Id–IIf***. However, when adding a rigid benzene ring in the azo compound ***If***, the length-to-breadth ratio of the obtained complexes was obviously improved which was of benefit to the mesogenic behaviour, thus relatively wide range of N* phase and TGBA* phase was found in the ***If***-derived H-bonded complexes. On the other hand, when the H-bonded donor was changed from only soft chain (***IIa***) to one rigid ring or two rigid rings in the structure, the length-to-breadth ratio was also increased. It was necessary to point out that the structure of naphthalene ring in the acid (***IIf***) not only increased the length of the molecule but also increased the width of the molecule. As a result, the aspect ratio of the molecule was not significantly improved, which could be confirmed by the phase transition points and the mesogenic behaviour of the complexes. In general, in the case of sufficient length-to-breadth ratio, the introduction of branched chain at the end of the azo compound or at the end of the carboxylic acid was an effective method to reduce the phase transition points of H-bonded LC complexes and shift the mesophase range around room temperature.

4. Conclusion

Five types of new pyridine-based azobenzenes, namely, 4-(4′-pyridylazo)-4′ ‘-alkoxybenzoates or 4-(4′-pyridylazo)-4’’-substituted benzoates were prepared as acceptors to construct mesogenic complexes with different H-bond donors. The formation and the stability of H-bonded supramolecular complexes were confirmed by FTIR spectroscopy. The mesophase behaviour of the H-bonded complexes was investigated and compared in detail. When the terminal chain of azo accepter or acid donor was changed from straight chain to branched chain, the length-to-breadth ratio of the resulting H-bonded complexes reduced accordingly. The H-bonded complexes with straight terminal were found to be mesomorphic, while only part of the azo-derived complexes with branched terminal showed mesogenic behaviours. When the H-bonded donor was changed from only soft chain to one rigid ring or two rigid rings in the structure, the length-to-breadth ratio was also increased, which could make the phase transition points increase and mesogenic properties extend.

Disclosure statement

No potential conflict of interest was reported by the authors.

Funding

This work was supported by the National Natural Science Foundation of China (Grant No. 61370048, 51333001, 51373024, 51473020) and the Fundamental Research Funds for the Central Universities: [Grant No. FRF-TP-15-003A3].

References

[1] Wolf JR, Dyer DJ. Hydrogen bonded liquid crystalline heterodimers incorporating alkoxystilbazoles and alkoxy-4-pyridones. Liq Cryst Today. 2015;24(2):47–55.
[2] He WL, Pan GH, Yang Z, et al. Wide blue phase range in a hydrogen-bonded self-assembled complex of chiral fluoro-substituted benzoic acid and pyridine derivative. Adv Mater. 2009;21(20):2050–2053.

[3] Miranda MD, Chávez FV, Maria TM, et al. Self-assembled liquid crystals by hydrogen bonding between bipyridyl and alkylbenzoic acids: solvent-free synthesis by mechanochemistry. Liq Cryst. 2014;41(12):1743–1751.
[4] Paleos CM, Tsiourvas D. Supramolecular hydrogen-bonded liquid crystals. Liq Cryst. 2001;28(8):1127–1161.
[5] Odinokov SE, Mashkovsky AA, Glazunov VP, et al. Spectral manifestations of intermolecular and interionic hydrogen bonding in adducts of various acids with pyridine. Spectrochimica Acta Part A Mol Spectros. 1976;32(6):1355–1363.
[6] Naoum MM, Fahmi AA, Refaie AA, et al. Novel hydrogen-bonded angular supramolecular liquid crystals. Liq Cryst. 2012;39(1):47–61.
[7] Fukumasa M, Kato T, Uryu T, et al. The simplest structure of the hydrogen-bonded mesogen built from 4-alkoxybenzoic acid and 4-alkylpyridine. Chem Lett. 1993;22(1):65–68.
[8] Lin HC, Shiaw JM, Wu CY, et al. Fused-ring and linking group effects of proton donors and acceptors on simple H-bonded liquid crystals. Liq Cryst. 2000;27(8):1103–1112.
[9] Kato T, Frechet JMJ, Wilson PG, et al. Hydrogen-bonded liquid crystals. Novel mesogens incorporating nonmesogenic bipyridyl compounds through complexation between hydrogen-bond donor and acceptor moieties. Chem Mater. 1993;5(8):1094–1100.
[10] Tong X, Wang G, Zhao Y. Photochemical phase transition versus photochemical phase separation. J Am Chem Soc. 2006;128(27):8746–8747.
[11] Sastry SS, Rao CN, Vishwam T, et al. Conformational studies of intermolecular hydorgen bonding through induced crystal G phase in nBA:7HB. Liq Cryst. 2013;40(7):932–941.
[12] Lee JH, Jang I, Hwang SH, et al. Self-assembled discotic nematic liquid crystals formed by simple hydrogen bonding between phenol and pyridine moieties. Liq Cryst. 2012;39(8):973–981.
[13] Lee JH, Lee HJ, Lee SJ, et al. Preparation of conjugated polymeric columns with a hexagonal symmetry from star-shaped supramolecular liquid crystals. Liq Cryst. 2013;40(1):112–119.
[14] Kihara H, Kato T, Uryu T, et al. Supramolecular liquid-crystalline networks built by self-assembly of multifunctional hydrogen-bonding molecules. Chem Mater. 1996;8(4):961–968.
[15] Yang F, Yuan J, Li C, et al. Novel triphenylene derivatives with acylthiosemicarbazide group: studies the influence of multiple H-bonding on mesomorphic properties. Liq Cryst. 2013;41(1):137–143.
[16] Kato T, Fréchet JMJ. New approach to mesophase stabilization through hydrogen-bonding molecular interactions in binary mixtures. J Am Chem Soc. 1989;111(22):8533–8534.
[17] Kumar U, KatoJ T, Fréchet MJ. Use of intermolecular hydrogen bonding for the induction of liquid crystallinity in the side chain of polysiloxanes. J Am Chem Soc. 1992;114(17):6630–6639.
[18] Pfletscher M, Wölper C, Gutmann JS, et al. A modular approach towards functional supramolecular aggregates–subtle structural differences inducing liquid crystallinity. Chem Commun. 2016;52(55):8549–8552.
[19] Chen Y, Yu H, Zhang L, et al. Photoresponsive liquid crystals based on halogen bonding of azopyridines. Chem Commun. 2014;50(68):9647–9649.
[20] Ahmed HA, Naoum MM. Mesophase behaviour of azobenzene-based angular supramolecular hydrogen-bonded liquid crystals. Liq Cryst. 2016;43(2):222–234.
[21] Alaasar M. Azobenzene-containing bent-core liquid crystals: an overview. Liq Cryst. 2016;43(13–15):2208–2243.
[22] Wang G, Zhang M, Zhang T, et al. Photoresponsive behaviors of smectic liquid crystals tuned by an azobenzene chromophore. RSC Advances. 2012;2(2):487–493.
[23] Alaasar M, Poppe S, Dong Q, et al. Mirror symmetry breaking in cubic phases and isotropic liquids driven by hydrogen bonding. Chem Commun. 2016;52(96):13869–13872.
[24] White TJ, Bricker RL, Natarajan LV, et al. Phototunable Azobenzene Cholesteric Liquid Crystals with 2000 nm Range. Adv Funct Mater. 2009;19(21):3484–3488.
[25] Zheng ZG, Li Y, Bisoyi HK, et al. Three-dimensional control of the helical axis of a chiral nematic liquid crystal by light. Nature. 2016;531(7594):352–356.
[26] Wang Y, Li Q. Light-driven chiral molecular switches or motors in liquid crystals. Adv Mater. 2012;24(15):1926–1945.
[27] Ma J, Li Y, White T, et al. Light-driven nanoscale chiral molecular switch: reversible dynamic full range color phototuning. Chem Commun. 2010;46(20):3463–3465.
[28] Liu HY, Wang CT, Hsu CY, et al. Optically tuneable blue phase photonic band gaps. Appl Phys Lett. 2010;96:121103.
[29] Chen XW, Wang L, Li CY, et al. Light-controllable reflection wavelength of blue phase liquid crystals doped with azobenzene-dimers. Chem Commun. 2013;49(86):10097–10099.
[30] Jin O, Fu D, Wei J, et al. Light-induced wide range color switching of liquid crystal blue phase doped with hydrogen-bonded chiral azobenzene switches. RSC Advances. 2014;4(54):28597–28600.
[31] Wang J, Shi Y, Yang K, et al. Stabilization and optical switching of liquid crystal blue phase doped with azobenzene-based bent-shaped hydrogen-bonded assemblies. Rsc Advances. 2015;5(82):67357–67364.
[32] Yin L, Wu Y, Gao J, et al. Optically binary liquid crystalline blue phases induced by one-armed cholesterol-linked azobenzene molecules. Soft Matter. 2015;11(30):6145–6151.
[33] Kim D-Y, Lee S-A, Park M, et al. Remote-controllable molecular knob in the mesomorphic helical superstructures. Adv Funct Mater. 2016;26(24):4242–4251.
[34] Tazuke S, Kurihara S, Ikeda T. Amplified image recording in liquid crystal media by means of photochemically triggered phase transition. Chem Lett. 1987;16(5):911–914.
[35] Ruslim C, Ichimura K. Conformational effect on macroscopic chirality modification of cholesteric mesophases by photochromic azobenzene dopants. J Phys Chem B. 2000;104(28):6529–6535.
[36] Bisoyi HK, Li Q. Light-driven liquid crystalline materials: from photo-induced phase transitions and property

modulations to applications. Chem Rev. 2016;116 (24):15089–15166.
[37] He W-L, Wang X, Yang Z, et al. Effect of the dimeric H-bonded mesogens of chiral acids on the mesogenic and optical properties. Liq Cryst. 2016;43(7):874–885.
[38] He W-L, Wei M-J, Yang H, et al. Flexible H-bonded liquid-crystals with wide enantiotropic blue phases. Phys Chem Chem Phys. 2014;16(12):5622–5626.
[39] He W-L, Huang Q, Yang Z, et al. Effect of bent-shape and calamitic-shape of hydrogen-bonded mesogens on the liquid crystalline properties. Liq Cryst. 2015;42 (8):1191–1200.
[40] Martínez-Felipe A, Imrie CT. The role of hydrogen bonding in the phase behaviour of supramolecular liquid crystal dimers. J Mol Struct. 2015;1100:429–437.
[41] Abdy MJ, Murdoch A, Martínez-Felipe A. New insights into the role of hydrogen bonding on the liquid crystal behaviour of 4-alkoxybenzoic acids: a detailed IR spectroscopy study. Liq Cryst. 2016;43(13–15):2191–2207.
[42] Paterson DA, Martínez-Felipe A, Jansze SM, et al. New insights into the liquid crystal behaviour of hydrogen-bonded mixtures provided by temperature-dependent FTIR spectroscopy. Liq Cryst. 2015;42(5–6):928–939.
[43] Martínez-Felipe A, Cook AG, Wallage MJ, et al. Hydrogen bonding and liquid crystallinity of low molar mass and polymeric mesogens containing benzoic acids: a variable temperature Fourier transform infrared spectroscopic study. Phase Transit. 2014;87 (12):1191–1210.
[44] Martinez-Felipe A, Cook AG, Abberley JP, et al. An FT-IR spectroscopic study of the role of hydrogen bonding in the formation of liquid crystallinity for mixtures containing bipyridines and 4-pentoxybenzoic acid. RSC Advances. 2016;6(110):108164–108179.
[45] Mallia VA, Antharjanam PKS, Das S. Synthesis and studies of some 4-substituted phenyl-4′-azopyridine-containing hydrogen-bonded supramolecular mesogens. Liq Cryst. 2003;30(2):135–141.
[46] Song X, Li J, Zhang S. Supramolecular liquid crystals induced by intermolecular hydrogen bonding between benzoic acid and 4-(alkoxyphenylazo) pyridines. Liq Cryst. 2003;30(3):331–335.
[47] Hedvati L, Nudelman A, Falb E, et al. Cinnamic acid derived oxazolinium ions as novel cytotoxic agents. Eur J Med Chem. 2002;37(7):607–616.